Wystąpienia pracowników ITME na konferencjach

C-MRS International '90
Beijing 18-22.06.1990 r.

J. SARNECKI, S.M. PIETRUSZKO*, A. SIENNICKI*
INSTYTUT TECHNOLOGII MATERIAŁÓW ELEKTRONICZNYCH
ul. Wólczyńska 133, 01-919 Warszawa

*INSTYTUT MIKROELEKTRONIKI I OPTOELEKTRONIKI PW
ul. Koszykowa 75, 00-662 Warszawa

CARIER LIFETIME IMPROVEMENT IN SILICON EPITAXIAL LAYER DUE TO LASER DAMAGE GETTERING

ZWIĘKSZENIE CZASU ŻYCIA W EPITAKSJALNEJ WARSTWIE Si W WYNIKU ZEWNĘTRZNEGO GETEROWANIA LASEROWEGO

Zastosowano mikroobróbkę laserową spodniej części podłożowych płytek Si, umożliwiającą wytworzenie w płytce trwałego układu naprężeń działającego getterująco na defekty punktowe i zanieczyszczenia metaliczne (Laser Backside Damage Gattering).

Krzemowe płytki podłożowe, silnie domieszkowane Sb, zostały poddane przed procesem epitaksji działaniu impulsów lasera Nd:YAG o gęstości energii zmienianej w zakresie 15-30 J/cm^2.

Określono wpływ mikroobróbki laserowej podłoża na czasy życia nośników mniejszościowych w epitaksjalnych warstwach Si o rezystywności 2-4 $\Omega \cdot cm$. Pomiary czasów życia przeprowadzono metodą Zerbsta z charakterystyk C-t kondensatora MOS.

Skuteczność zewnętrznego getterowania laserowego określono przez porównanie czasów życia nośników mniejszościowych warstw na podłożach poddanych działaniu impulsu lasera i na podłożach bez mikroobróbki laserowej. Zaobserwowano 2-3 krotny wzrost czasów życia nośników mniejszościowych w warstwach osadzanych na podłożu po laserowej mikroobróbce.

Określono zmiany czasów życia w funkcji głębokości obszaru zubożonego.

Wystąpienie będzie opublikowane w materiałach z konferencji C-MRS International'90

Second International Conference on the New Diamond Science a.id Technology
Washington 23-27.09.1990 r.

A. SZYMAŃSKI, L. HOZER, A. NIEDBALSKA
INSTYTUT TECHNOLOGII MATERIAŁÓW ELEKTRONICZNYCH
ul. Wólczyńska 133, 01-919 Warszawa

MULTISEEDS HP/HT LPE* OF DIAMOND

1. INTRODUCTION

On the basis of applied mineralogy, in contrary to the majority of geologists and technologists, we are convinced that most of the hypotheses on the diamond formation in Nature (product of magma crystallization in the very deep region of the mantle) are seemingly true only.

Our genetic analysis of natural and synthetic diamond nucleation and growth as well as experiments, especially programmed from the precursor raw materials preparation up to HP/HT synthesis, confirm that opinion (Niedbalska, 1987; 1988; 1989b; Niedbalska and Szymański 1987; 1990; Szymański 1990). In accordance with the earlier studies (Badzian, 1984; Badzian and Badzian, 1980; Bundy, 1963; Dawson, 1980; Goodman, 1987; Kropotova et al., 1967; Schmalzried, 1974; Sobolev and Shatsky, 1986; Stoch, 1987; 1989; Strand, 1986; Wiereszczagin et al., 1977) we set down the scheme of the nine possible mechanisms of the diamond pha e nucleation and growth (Fig. 1).

The graphite/diamond equilibrium plot for eclogites (line C in Fig. 2) proved that industrial process of HP/HT static diamond synthesis - graphite to diamond transformation in a presence of metallic solvent/catalyst (equilibrium line A, Fig. 2) in the temperature above 1500 K - is technically strained by the pressure, probably much exceeding that in natural conditions in the mantle. Increasing the pressure of synthesis was the fastest way for industrial progress from the thirties and in such circumstances physicochemical knowledge of the precess receded into the background.

Most of the synthetic diamonds, commercially produced, were grown from the graphite in the presence of solvent/catalyst metals. Maximal grain sizes, possible to obtain in that way, are up to 1 mm, when the shape is isometric. The growth process is determined by the carbon solubility and diffusivity difference on the graphite/metal and diamond/metal interfaces.

Wentorf (1971) has proposed a reconstitution technique for promoting a growth of the large diamond crystals. In that process small diamonds are used as a source of carbon in sp^3 configuration for the on-seed-growing stones. Diamonds are dissolved in a hot zone of solvent/catalyst and the diamond stone grows in a cold zone, where the seed crystal is placed. Solubility difference of carbon, depending on temperature

*LPE - Liquid Phase Epitaxy

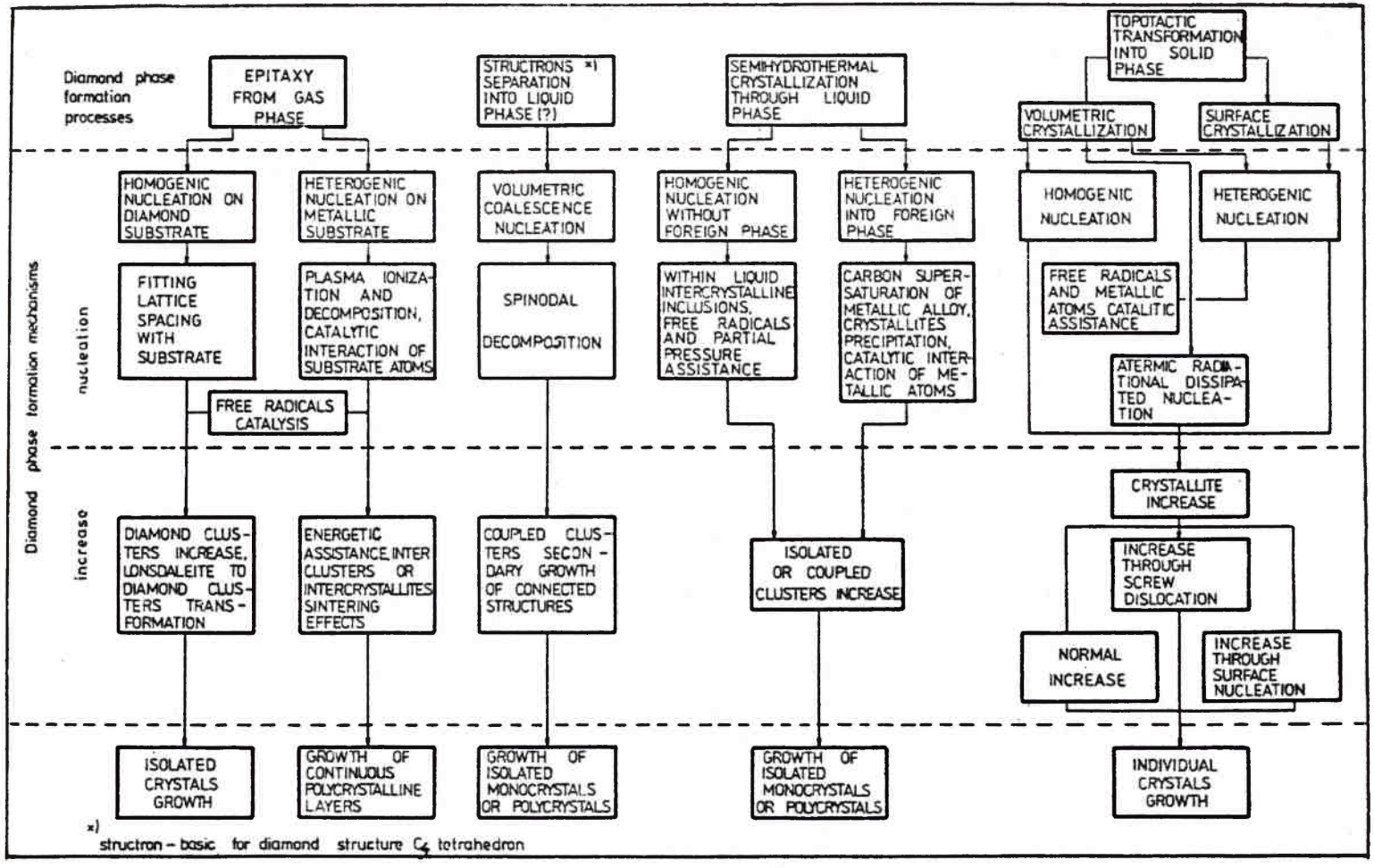

Fig. 1. Theoretically possible mechanism of nucleation and growth of diamond crystals in dependence on precursor raw materials state of aggregation and catalytic factors of the process.

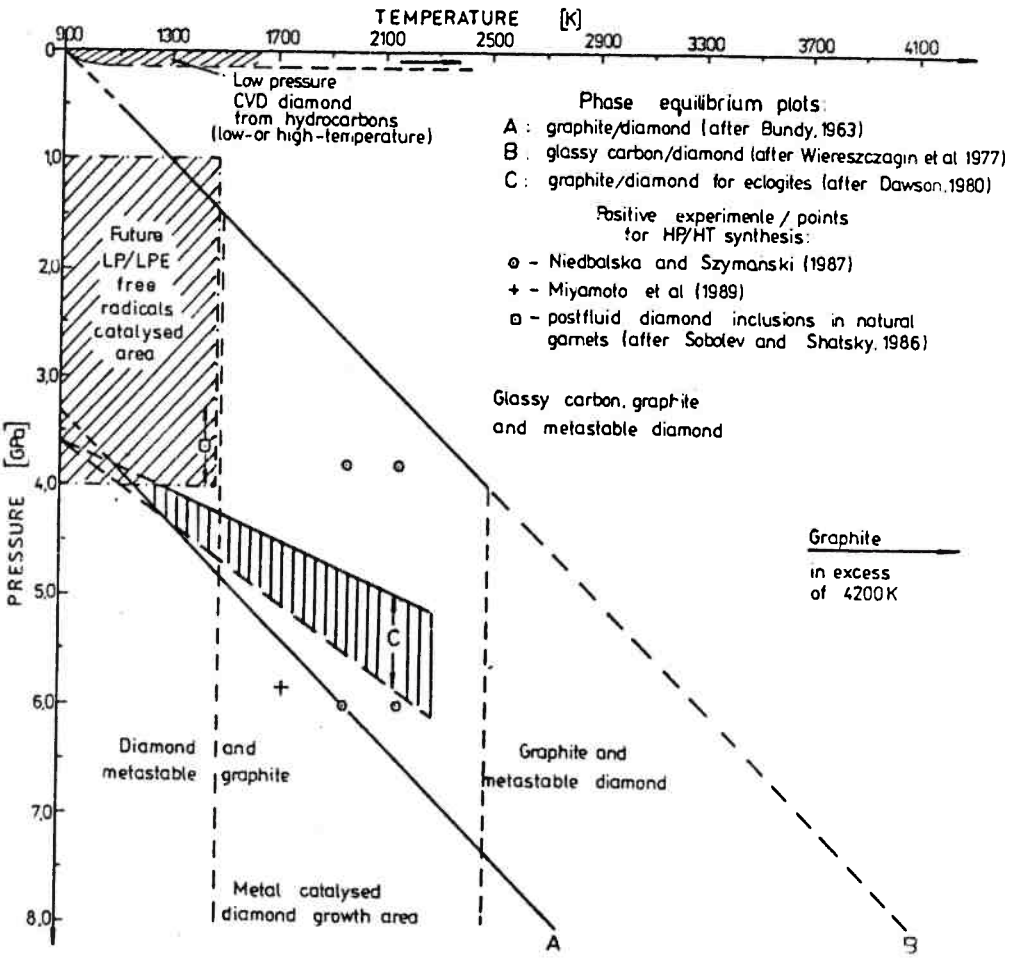

Fig. 2. Pressure-temperature equilibrium lines for different carbon precursors to diamond

is thought to be a driving force for the diamond crystal growth. The orientation of the grown stone may be controlled by positioning of the seed diamond. The habit of the grown stone depends, as in Nature, on the synthesis conditions (Burns, 1988; Sunagawa, 1984). The lower temperature and the higher pressure make the cubic habit diamonds growth more likely than the octahedral. Burns (1988), applying the reconstitution technique and controlling the axial temperature gradient at the constant pressure obtained large synthetic diamonds, weighting up to 11 cts. Crystal quality was good for drawings, radiation detectors and thermoluminescent dosimeters. Sumitomo Electric (1989) claims to be able to mass-produce single crystal diamonds weighting 5÷9 cts for electronics, cutting tools and ultra-hard scalpels. The concept of reconstitution process of the large diamond stones growth is similar to the principles of the hydrothermal quartz growth in industrial processes. Niedbalska (1987) has named it 'semihydrothermal process of diamond growth in the liquid metallic alloy".

2. LOW PRESSURE STATIC DIAMOND SYNTHESIS

In our experimental synthesis processes, the applied pressure was approximately 1,2 GPa higher or lower than that for Dawson's (1980) equilibrium conditions (line C in Fig. 2). Our positive results, for the first time presented at the XXV EHPRG Congress (Niedbalska and Szymański, 1987) were in the same time verified by Sobolev and Shatsky (1986) who found diamond microcrystals grown as a result of metamorphic carbonization, nucleation and LPE in liquid hydrocarbons environment closed as a bubble inclusions in a garnet crystals. These microcrystals grew under the pressure of 3,5÷4 GPa, as it is known from investigated metamorphic rocks genesis.
The conditions of diamond growth, given by Sobolev and Shatsky are close to the Dawson equilibrium line and lie between A (graphite/diamond) and B (glassy carbon/diamond) equilibrium lines.

Our experiments of diamond synthesis from the glassy carbon under the high pressure, were verified recently by Miyamoto et al. (1989) (Fig. 2 and 3). Onodera et al. (1988) also synthetized diamonds from the glassy carbon precursor, however pressure applied in their experiments exceeded 10 GPa. Thus, in these processes graphitization of the whole glassy carbon preceded diamond nucleation (Fig. 3). In the Fig. 3 we drafted two types of different areas: T_S/P (temperature of synthesis) and T_C (temperature of carbonization of organic compound being the substrate for the glassy carbon precursor). All discussed experiments (Niedbalska and Szymański, 1987; 1989a; Onodera et al., 1988; Miyamoto et al., 1989) were carried out using the glassy carbon precursors, annealed in the similar temperatures T_C.

In the early studies (Wentorf, 1965; Hirano et al., 1982; Näka et al., 1984; Novikov et al., 1987), the high-temperature-carbonized (T> 1880 K) glassy carbon was used. In this case the glassy carbon content sp^2 orbitals and the bulk transformation to graphite in HP process with mettalic catalyst is to be expected.
Sobolev and Shatsky's (1986) diamonds can be shown in two regions in Fig. 3: T_S/P and $(T_C + T_E)/P$ (T_E - temperature of epitaxy). The latter one is more logical and in this

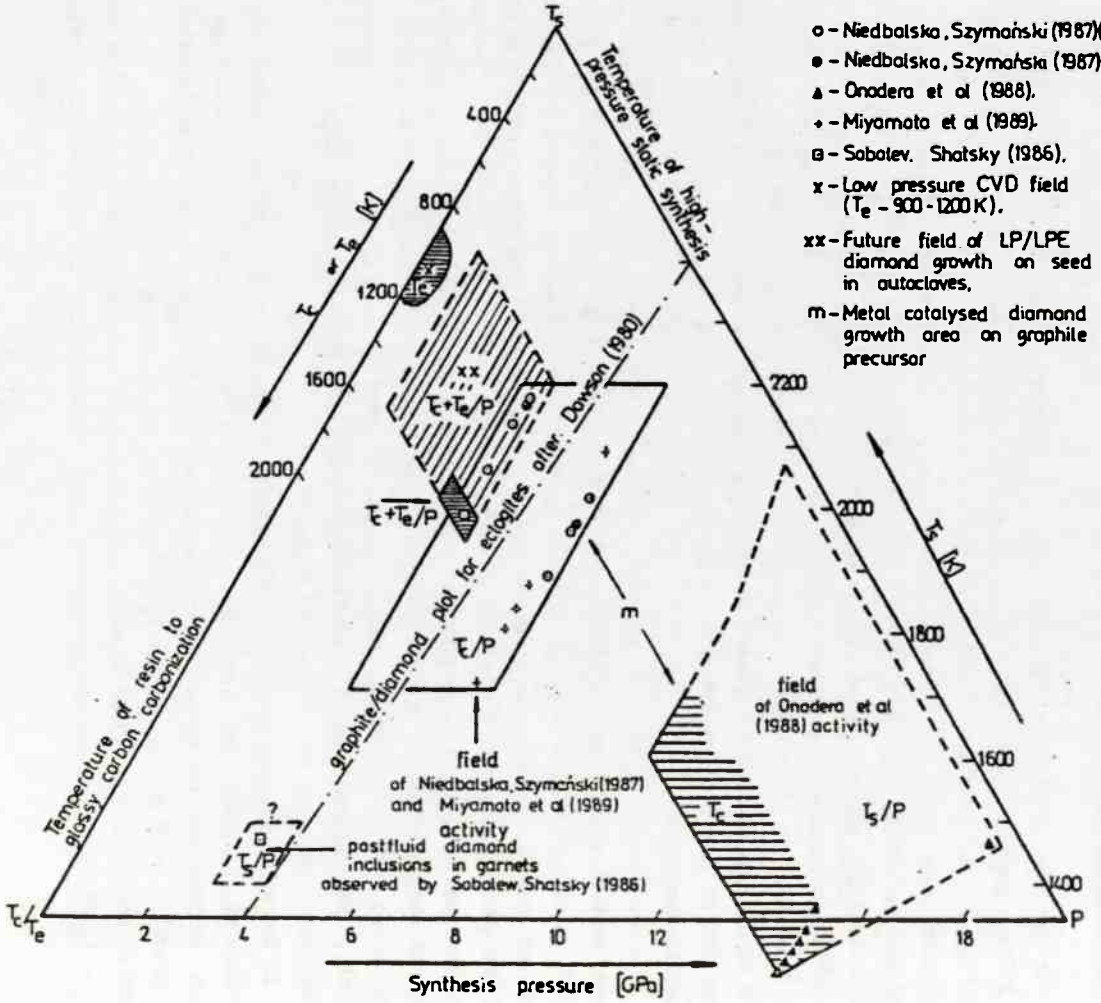

Fig. 3.

Triaxial T_C/T_E - T_S - P system of diamond nucleation and growthin Nature and in a laboratory.
T_C - temperature of dense organic precursor carbonization,
T_E - temperature of hydrocarbon decomposition and CVD diamond nucleation and growth, T_S (T_S/P) - temperature of diamond high pressure static synthesis, T_E/P - LPE (liquid phase epitaxy) through metal catalyst under high pressure, LPLPE - low pressure liquid epitaxy

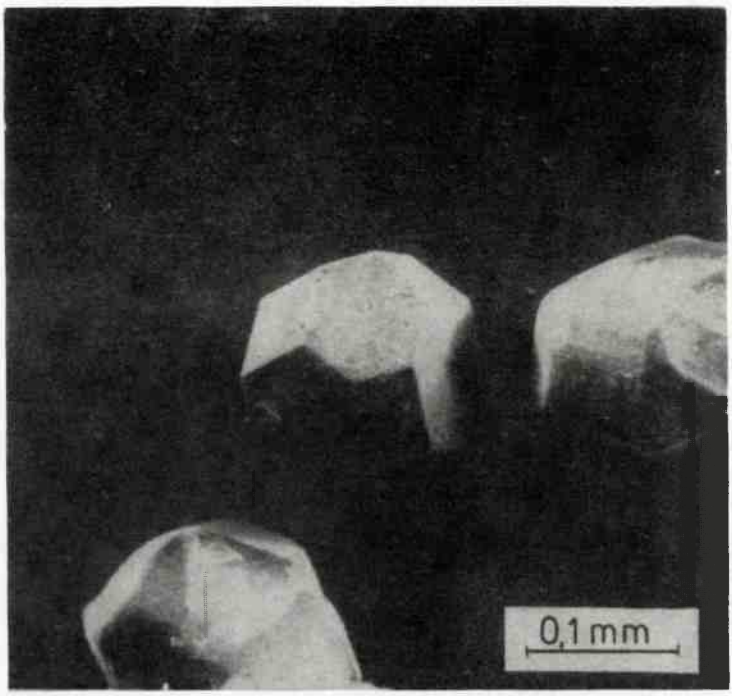

Fig. 5. Colorless diamond crystals synthetized at 2170 K and low pressure of 3,8 GPa

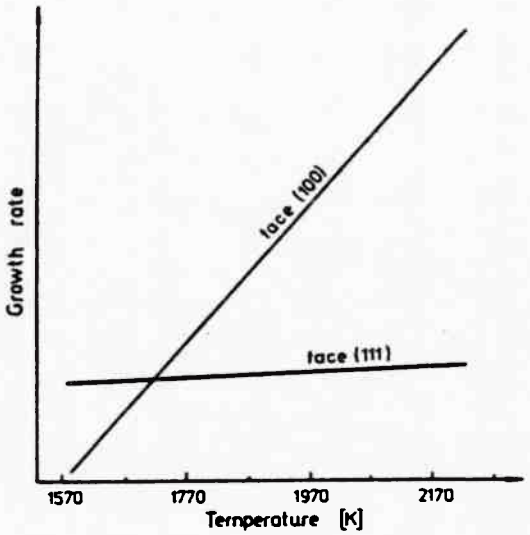

Fig. 4. A schematic temperature dependency of the growth rate of (111) and (100) faces of diamond crystals (Sunagawa, 1984)

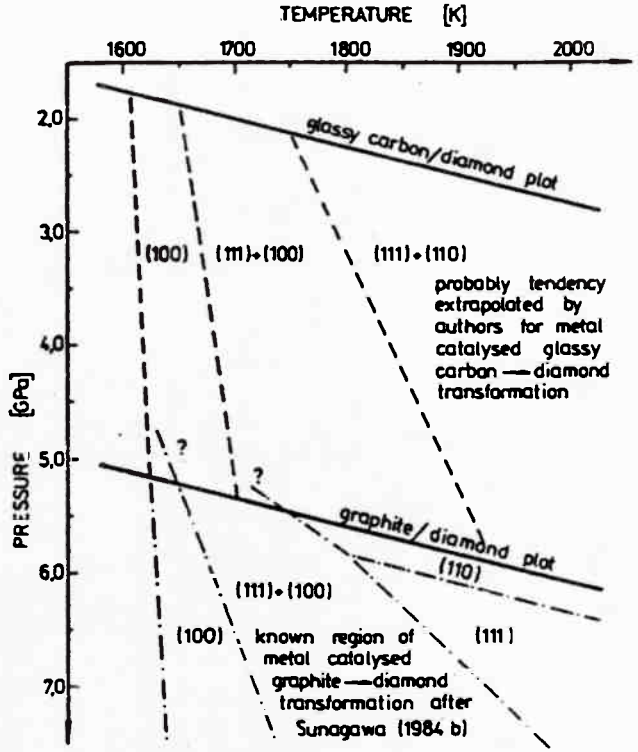

Fig. 6. Morphodrom of synthetic diamond (after Sunagawa, 1984) extrapolated to lower pressure region of metal-catalyzed diamond synthesis from a glassy carbon precursor

case it would support our suggestion that future development of HP/HT synthesis (especially on-seed diamond growth) will be based on epitaxy phenomena - as we have shown in Fig. 2 and 3 (lined T_E/P areas). It will be low-pressure liquid phase epitaxy (LPLPE).

The temperatures of our syntheses were chosen according to the Sunagawa (1984) prediction on the (111) and (100) faces growth rates shown in Fig. 4. In order to obtain the maximal (100) face growth rate the temperature was much higher than 1800 K (approximately 1970 and 2170 K). All of the our diamond crystals are cubooctahedrons with well developed (100) faces and equipondement or underdeveloped (111) faces (Fig. 5). In some crystals the beginning of the (110) faces formation was sporadically observed. This was also verified by morphodrom of synthetic diamond (Fig. 6). Morphodrom of the known process of the metal catalyzed diamond synthesis from graphite, given by Sunagawa (1984) must be modified for considering the synthesis from glassy carbon. However, up to now experiments show the tendency only. Analysis of this tendency and its extrapolation suggest that decrease of the synthesis pressure in the same temperature range should gradually prefer cubooctahedral and octahedral crystal growth. This is the case where most of the CVD processes are placed (Johnson et al., 1988; Szymański, 1989b).

3. THE MECHANISM OF A TWO-COMPONENT SYSTEM NUCLEATION AND GROWTH

If, the initial composition is selected in the metastable region as x_o with a corresponding free energy of G_o, where small volume of the new phase (embryos) is formed with different composition x_E and free energy G_E, then formation of a certain volume of the new phase leads to a change in the initial composition from x_o to x_M as depicted in Fig. 7, showing the free energy of an atom (molecule) plotted as a function of the atomic (mole) fraction of the binary solution. If the lever rule is employed to express the relative amounts of separated phases, then the change in the free energy per unit volume of the new phase formed from homogeneous composition x_o can be expressed as

$$\Delta G_v = \frac{1}{\bar{V}} \left(\frac{x_o - x_M}{x_E - x_M} G_E + \frac{x_E - x_o}{x_E - x_M} G_M - G_o \right) \frac{x_E - x_M}{x_o - x_M}, \qquad (1)$$

where $\bar{V}$ is the mean value of the volume of an atom (molecule) in the new phase. Rearrangement of equation (1) yields

$$\Delta G_v = \frac{1}{\bar{V}} \left[G_E - G_M - \frac{x_E - x_M}{x_o - x_M} (G_o - G_M) \right]. \qquad (2)$$

As the difference in the composition of the initial phase $x_o - x_M$ and the corresponding free-energy difference $G_o - G_M$ are small, Eq. (2) can further be modified to give

$$\Delta G_v = \frac{1}{\bar{V}} \left[G_E - G_M - (x_E - x_o) \left(\frac{dG}{dx} \right) x_o \right]. \qquad (3)$$

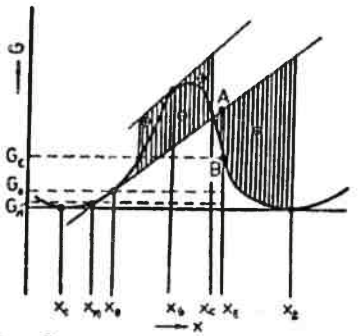

Fig. 7

Graphical depiction of the driving force for liquid phase separation in a two-component system, considering the mechanism of nucleation and growth for an initial composition of (x_0) and considering spinodal decomposition for an initial composition of (x_S) (Strand, 1986)

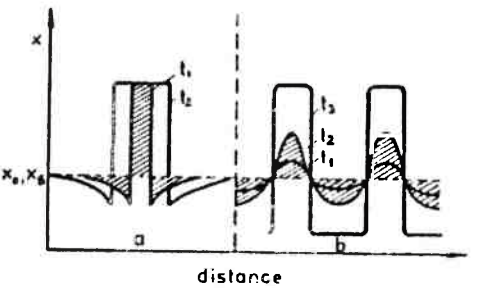

Fig. 8

Schematic change and development of concentration profile along distance axis:
a - for homogenic nucleation and growth,
b - for spinodal decomposition and growth;
t_1, t_2, t_3 - time ($t_3 > t_2 > t_1$),
x - concentration, x_0 and x_S - average concentrations (Schmalzried, 1974; Strand, 1986)

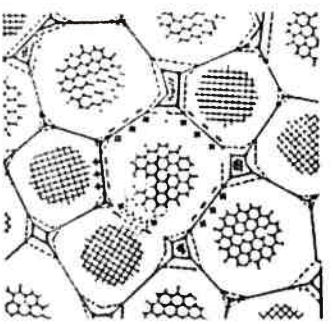

Fig. 9

Representation of a two polymorph strainded mixed cluster random network glass at a low temperature when all residual is frozen out. On the cluster corners last liquid or hypereuthectic phase may be frozen (Goodman, 1987)

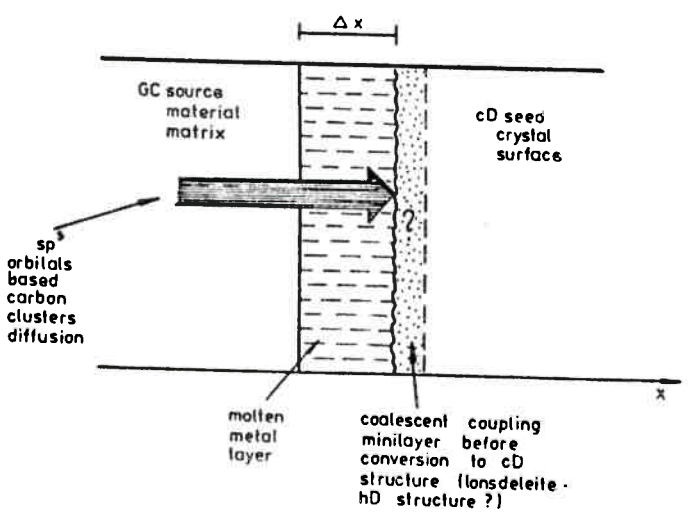

Fig. 10

Schematic structure of the sp^3 organized carbon diffusion of the interface of the diamond seed crystal

It follows from the geometry of Fig. 7 that

$$\Delta G_v = \frac{1}{V} [\overline{AB}], \tag{4}$$

where $\overline{AB}$ represents the value of the driving force for nucleation of the new phase with composition x_E, which is given in general by the vertical segment limited by the point on the free energy curve for the corresponding nucleus composition (G_E) and the intercept with the tangent to the free-energy curve at the initial composition (x_o). It is apparent from equation (4) that, provided that segment AB lies above the G(x) curve, the value of the driving force is positive and, if it lies below the curve, than the value is negative. The regions of the new phase with composition $x_E < x_C$ will thus have a negative driving force, which becomes positive when $x_E > x_C$ and attains a maximum at equilibrium composition x_2.

Thus, finite changes in the composition between x_C and x_2 are necessary for the formation of stable regions of the new phase (nuclei) from initial composition x_o, in order for further growth to occur, assuming that their size attains a critical value, determined by the interfacial energy of the initial and new phases. Thus the mechanism of nucleation and growth is considered for formation of a new phase for an initial composition lying in the metastable region.

Aforementioned mechanism of classical nucleation describes homogeneous, uniform nuclei with the composition of the equilibrium phase grown from supersaturated melt (Fig. 8a). Experimentally was found another way of lowering solution supersaturation - spinodal decomposition. In such a process coherent decomposition in a long time, without distinct phase boundary, takes place (Fig. 8b). If the initial concentration lies in the spinodal region (Fig. 7) decomposition occurs as a result of continuous composition changes in the bulk of solution. For thus non-uniform nucleation Cahn and Hilliared (1958, 1959) used equation

$$G = \int_V [g(x) + k(\nabla x)^2 + \ldots] dV, \tag{5}$$

where G is the overall from energy per unit volume, g(x) is the free energy per unit volume in a homogeneous system with composition x and expression $k(\nabla x)^2$ is the first term in the expression representing the growth in the free energy as a result of the composition gradient and can be connected with the energy for formation of a phase boundary.

This equation (5) is valid for any concentration fluctuation and thus can be used for nucleation. It can be used for calculation of the properties of the nuclei without assuming their homogeneity and also does not require separation of the energy of the nuclei into surface and volume contributions. After treatment of equation (5) we may calculate the change in free energy between the original homogeneous solution and a solution where the composition at each point differs little from the average composition x_S and changes with a small concentration gradient,

$$G = \int_V \left[\frac{1}{2} \frac{\partial^2 g}{\partial x^2} (x - x_S)^2 + k(\nabla x)^2 \right] dV. \tag{6}$$

If concentration fluctuations are expressed by the relationship

$$x - x_s = A \cos \beta \phi \quad , \tag{7}$$

where $\beta = 2\pi/\mu$ and where β is the wave number, A is the amplitude, ϕ is a distrubution parameter and μ is the wavelength of the fluctuation, than the contribution of ΔG to this fluctuation can be expressed as

$$\Delta G = \frac{A^2}{4}\left[\left(\frac{\partial^2 g}{\partial x^2}\right)_{x_s} + 2k\beta^2\right]. \tag{8}$$

As the value of k is positive (otherwise a negative surface tension would result with no stability even outside the spinodal) for systems with a tendency to separate, it is apparent from equation (8) that ΔG is positive if $(\partial^2 g/\partial x^2)_{x_s}$, i.e. if x_o lies outside the spinodal region.

Spinodal decomposition was observed in liquids of high viscosity, metals, ionic crystals and glasses. Similar, characteristic continuous meander structures were observed in domains in magnetic crystals (Szymański, 1989a), however this can also result from the mechanism of embrionucleation and growth through coalescence processes at high nucleation rates and with a large content of the separated new phase (spontaneous nucleation?).

Spinodal decomposition as a non-uniform, non-homogeneous nucleation seems to be in a good correlation with a new concept of a glassy structure formation, presented by Goodman (1987) and named "the strained mixed cluster model" (Fig. 9). Supercooled liquid contains loose nanometric clusters (or structrons - Fig. 1) in the disorganized structure. According to Goodman, glass structure may be formed in a system which:

1.- show at last two polymorphic forms in the solid state,
2.- the polymorphic forms must not be capable of forming low strain interfaces with each other,
3.- bond strength should be high, but the relevant elastic constants small.

All mentioned conditions are observed in the inorganic, oxide, sulfuric and metallic glasses. They also may be adapted to the glassy carbon used by us as precursor for diamond synthesis. Glassy carbon may in the same time contain nanometric graphite (three forms), hexagonal lonsdaleite or cubic diamond clusters on the carbon chain crossings in the form of embrionuclei.

The change in the system energy may induce a spontaneous devitrification in the glassy carbon analogous to the other glasses. As a result, different polymorphs of crystalline carbon nuclei may originate on the crossings of carbon chains. The polymorphic transformations of the nuclei are possible, depending on the time of the process. Formation of the nuclei may be catalyzed by admixture of metallic solvent (like for graphite raw material) or, similarly to the CVD process, self-catalysis by highly active free radicals (H^+, CH_3^+, $C_2H_5^+$, etc.) formed "in situ" during the mother resin decomposition.

Investigation of the similarity between HP diamond nucleation in the glassy carbon and conwentional devitrification of glasses as well as taking into consideration the possibility of the spinodal decomposition open new ways of interpretation of the HP/HT diamond synthesis processes.

Diffusion of atoms in solid state may also slow down the processes of diamond nucleation and growth. Badzian and Badzian (1980) synthetized a cubic BN crystals by the diffusion topotactic transformation in the solid state from a hexagonal BN powder, in a presence of an AlN catalyst, under pressure of 5 GPa and temperature of 1870 K. They showed that the hex BN ⟶ cub BN conversion could proceed without any intermediate liquid phase, in a process similar in its nature to the contact metamorphism. During crystallization the starting precursor (hex BN) and catalyst (AlN) undergo atomization.

As we may deduce from aforementioned discussion most probable natural environment for the good contoured diamond crystals growth are the liquid hydrocarbon filled microgeodes (Bundy, 1963; Smalley et al., 1985). Hydrocarbons are decomposed to carbon without metal catalyst but under the high isostatic partial pressure and the high temperature. By analogy we may consider industrial HP/HT static synthesis of diamond as "semihydrothermal" - metalothermal high pressure liquid phase epitaxy (MHPLPE). If we place the seed diamond crystal coated with metal catalyst layer the sp^3 orbitals organized carbon source (glassy carbon), diamond nucleation and growth may proceed continuously by the way of spinodal decomposition (Fig. 7 and 8) of carbon source, diffusion through liquid metal layer and volumetric coalescence on the seed crystal surface. Such a microchamber of the seed crystal surrounded with the liquid metal and the carbon source may be analyzed as the separated MHPLPE autoautoclave. In the typical chamber for HP/HT synthesis we may place charge composite prepared by the carbon source packing with aforementioned autoautoclaves.

The rate of on-seed-diamond growth is determined by the of diffusion process of sp^3 structrons through the molten metal layer onto the seed crystal interface, as shown in Fig. 10. The most important factors are: coefficient of diffusion of structrons - $D_{sp^3}C$, width of the metallic layer and the time of the diffusion. Question arises, what is a mechanism of on-seed-diamond growth. It can proceed directly from the as diffunded structrons or an intermediate layer of hexagonal diamond (lonsdaleite) is present.

As a result we suggest two ways of the future development of diamond crystal nucleation and growth (Fig. 2 and 3):

1.- "low pressure liquid phase epitaxy" (LPLPE),

2.- "solid state structrons separation" (SSSS) or in other words "spinodal decomposition and diffusional transformation" (SDDT). For solid solutions such a process is known as Ostwalo ripening.

The HP/HT diamond synthesis was not analyzed till now from the above point of view. The SDDT process we can locate between "very low pressure epitaxy" (VLPE=CVD) and "metalothermal high-pressure liquid phase epitaxy" (MHPLPE) - Fig. 2. For this process we must seek a novel catalytic compounds and analyze different physical phenomena (Hazen, 1990; Smalley, 1985).

4. FUTURE DEVELOPMENT OF HP/HT DIAMOND SYNTHESIS

If we assume that diamonds in Nature most probably grow from polymerized and decarbonized hydrocarbons (Niedbalska, Szymański, 1987; Niedbalska, 1988; Szymański, 1990) than Sunagawa's (1984) suggestion that "natural diamonds are not formed in metamorphic environments" is not a rule (Sobolev and Shatsky, 1986). Thus, we must analyze the future development of the HP/HT diamond synthesis taking into account different metamorphic processes occurring in the Earth mantle (Fukunaga et al., 1990; Krasoń et al., 1990).

Wentorf (1971) reconstitution technique confirmed with the good results by Burns (1988) as well as Kropotova et al. (1967) observations of isotrooic fractioning of carbon precipitation from hot methane gas ontc seed diamond all suggest the necessity of new thinking in projecting of the future diamond synthesis. This should happen especially when on-seed large stone growth is considered. Good technical properties of Burns colored stones as well as colorless crystals obtained by Niedbalska and Szymański (1987) and Niedbalska et al. (1988) lay down the direction of future development, up to good quality jeweller s type stones growth. Taking this way we must change:

1.- the manner of thinking about the process,
2.- environment of carbon dissolution,
3.- catalyzing agents,
4.- the process charge organization,
5.- the process chamber construction,
6.- the process realization time.

The first and the second of above points are most troublesome. The researchers should have an interdisciplinary education with good mineralogical-petrological as well as inorganic-organic chemistry knowledge. Additionally they must have knowledge of crystallography and thermodynamics as well as materials science.

The third point, especially the free radicals catalysis, was first investigated with chemical reactions in living structures and this kind of catalysis is utilized in organic chemistry. We believe that the free radicals will be effective in diamond synthesis from postorganic precursors (Rozpłoch, 1987; Niedbalska, 1988; Niedbalska and Szymański, 1990; Wadas, 1987). This should effect in future in lowering of the synthesis conditions (T, P) to the very low level.

Points four and five are very important as resulting from the basic knowledge of the process and usually determine the socalled "know-how" - not published and not patented.

The last, sixth point indicates that it is probable that the process of synthesis may last for a long time (14-20 days) under programmed pressure and temperature profile.

We are conducting, for a two years, a special HNSD program for simulation of seminatural process of the diamond stones growth in lowered HP/HT conditions (Hozer et. al., 1990).

5. BIBLIOGRAPHY

Badzian A. (1984) - Ph.D. Thesis; Pub: Prace ITME No. 12, Warszawa

Badzian A., Badzian I. (1980) - in High Pressure Science and Technology, Ed. by B. Vodar, P. Marteau, Pergamon Press, vol. 2, pp. 1087-1099

Bundy F. (1963) - J. Chem. Phys., 38(3) pp. 631-643

Burns R.C. (1988) - Abstr. 1st ICNOST, Tokyo, Oct. 24-26, No. 2-12

Cahn J.W., Hilliard J.E. (1958, 1959) - J. Chem. Phys., 28, p. 258, 31, p. 688

Dawson J.B. (1980) - Kimberlites and Thei Xenoliths, Springer-Varlag, Berlin, p. 179

Fukunaga O., Miyake M., Jizuka M., Miyamoto M., Niedbalska A., Szymański A. (1990) - Proc. XXVIII EHPRG, Bordeaux, In press

Goodman C. (1987) - Glass Technol., 28(1) pp. 19-28

Hirano S., Shimono K., Naka S. (1982) - J. Mat. Sci., 17, pp. 1856-1862

Hozer L., Niedbalska A., Szymański A. (1990) - Unpubl. data

Johnson G.H., Badzian A., Geis M.W., ed. (1988) - Diamond and Olamond-Like Materials Synthesis, Ext. Abstr., MRS Publ., Pittsburgh

Krasoń J., Savkevitch S., Szymański A. (1990) - Proc. 2nd ICNOST, Washington, In press

Kropotova O.J., Grinenko V.A., Bezrukov G.N. (1967) - Geochem. Int., 4pp. 819-820

Miyamoto M., Akaishi M., Ohsawa T., Yamaoka S., Fukunaga O. (1989) - J. Cryst. Growth 37, pp. 731-738

Naka S., Tsuzuki A., Hirano S. (1984) - J. Mat. Sci. 19, pp. 1153-1158

Niedbalska A. (1987) - Arch. Miner., vol. XLII (1) pp. 97-107

Niedbalska A. (1988) - Ph. D. Thesis; Pub: Prace ITME, No 28 (1989), Warszawa

Niedbalska A (1989a) - Proc. GAC-MAC-ICAM-CAM Conf., Montreal, May 14-17. Pub: Process Mineralogy IX: Application to Mineral Beneficiation, Metallurgy, Gold, Diamonds, Ceramics, Environment and Health (1990), pp. 615-620

Niedbalska A. (1989b) - Proc. XXVII EHPRG, Paderborn, July 17-21. Pub: High Pressure Res. vol 5, (1990), pp. 708-710

Niedbalska A., Szymański A. (1987) - Proc. XXV EHPRG, Potsdam, Aug. 25-27, High Pressure Geosciences and Materials Synthesis, vol. 17, (1988), pp. 34-37

Niedbalska A., Szymański A., Zalewski S.A. (1988) - Abstr. Ist. ICNOST, Tokyo, Oct. 24-26, No. 2-19

Niedbalska A., Szymański A., (1990) - Proc. XXVIII EHPRG, Bordeaux, In press

Novikov N., Fedoseev O., Shulzenko A., Bobatyreeva G. (1987) - Sintez Almazov, Naukova Dumka, Kijov, p. 279

Onodera A., Higashi K., Irie Y. (1988) - J. Mat. Sci. 23 pp. 422-428

Rozpłoch F. (1987) - Priv. Inf.

Schmalzried H. (1974) - Solid State Reactions, Verlag Chemie, Weinhein

Smalley R., Heath J., O'Brien S., Zhang Q., Lin Y., Curi R., Kroto H., Tittel F. (1985) - J. Amer. Ceram. Soc., 107, 7779-7780

Sobolev N.W., Shatsky W.S. (1986) - Geol. and Geoph., 7, pp. 77-80, Novosybirsk

Stoch L. (1987) - J. Thermal Anal., 32, op. 1651-1658

Stoch L. (1989) - Thermochimica Acta, 148, pp. 149-164

Strand Z. (1986) - Glass-Ceramic Materials, Elsevier, Amsterdam, pp. 46-53

Sumimoto Electric Ind. Ltd (1989) - Adv. Ceram. Rep., 4(11) p. 2

Sunagawa J. (1984) - in Mat. Sci. of Earth's Interior Terrapub., Tokyo, pp. 63-105, 303-330

Szymański A. (1989) - Technical Mineralogy and Petrography - An Introduction to Materials Technology, Elsevier, Amsterdam, vol. 1, pp. 508-524; vol. 2, tab. A.8

Szymański A. (1989b) - Proc. LS:5 Int. Symp. of Light Sources, York, 10-14 Sept., p. 61
Szymański A. (1990) - Proc. 15th IMA Meeting, Beijing, In press
Wadas R.S. (1987) - Monocrystallization Catalysis - Hypothesis, Unpublished
Wentorf R.H. (1965) - J. Phys. Chem., 69, pp. 3063-3069
Wentorf F.H. (1971) - J. Phys. Chem., 75, p. 1833
Wiereszczagin L., Jakovlev J., Buczkov L., Dymov W. (1977) - Tieplofiz. Vys. Temp., 15(2), pp. 316-321

IX Szkoła Fizyki i Zastosowań Monokryształów
i Materiałów Ciekłokrystalicznych
Jurata 22-29.10.1990 r.

P. KAMIŃSKI, W. STRUPIŃSKI
INSTYTUT TECHNOLOGII MATERIAŁÓW ELEKTRONICZNYCH
ul. Wólczyńska 133, 01-919 Warszawa

DEEP LEVEL STUDIES IN GaP:N,S EPITAXIAL LAYERS

GaP epitaxial layers doped with nitrogen and sulfur are used for manufacturing electroluminescent devices emitting yellow-green light. The main problem in obtaining high electroluminescent conversion efficiency is to control the concentration of of point defects which can act as non-radiative recombination centres. In this paper OLTS technique was applied to investigate the residual deep-level defects in VPE GaP:N,S. Three defect centres with activation energies for electron thermal emission of 0.24 eV, 0.28 eV and 0.44 eV were detected. The concentration of the 0.24-eV and 0.44-eV traps was found to be dependent on substrate temperature. Experimental evidence is given that the 0.24-eV-trap, related to phosphorus vacancy, has a detrimental effect on radiative recombination efficiency in the epitaxial layers.

I. INTRODUCTION

Vapour Phase Epitaxy (VPE) is widely used for growing thin layers of the III-V compound semiconductors which are applied in optoelectronics for the fabrication of Light-Emitting Diodes (LEDs) and displays. Epitaxial gallium phosphide doped with nitrogen and sulfur is a starting material for efficient sources of green or yellow-green light. Nitrogen is an isoelectronic impurity in GaP and it acts as the efficient radiative recombination centre. The radiation is generated due to the decay of excitons bound to nitrogen atoms [1]. The concentration of sulfur determines the Fermi level position.

The radiative recombination of excess charge carriers is, however, accompanied by the nonradiative recombination resulting from deep defect centres which are mainly related to the point defects generated during the growth of the epitaxial layer. These defects have not been established yet, though there are some experimental data [2-4] showing that the nonradiative recombination centres can be attributed to Ga vacancies, deep impurities such as Cu or Fe and complexes: V_{Ga}-O_P, $(V_{Ga})_2$-P_{Ga}, C_{Ga}-O_P and Si_{Ga}-O_P. Stringfellow and Hall [5] have shown that luminescent properties of VPE GaP can be strongly affected by a change in the ratio of $[A^{III}]/[B^{V}]$ where $[A^{III}]$ is the group III component concentration and $[B^{V}]$ is the group V component concentration in the gas phase. They have found that the minority carrier lifetime obtained from the photoluminescent decay measurements increases from 10 to 100 ns with increasing

the ratio of the partial pressures in the input gas stream $P^o_{HCl}/P^o_{PH_3}$ from 0.3 to 10. This result, obtained for the growth temperature of 840°C, was correlated with the improvement of the LEDs output. Stringfellow and Hall [5], however, have not monitored the changes in the material defect structure and it is not clear whether the improvement of quantum efficiency was due to a diminution of the V_{Ga} concentration or due to an increse in the nitrogen concentration.

In the present work, we employed Deep Level Transient Spectroscopy (DLTS) to monitor a change in the defect structure of VPE GaP:N,S resulting from an increase of substrate temperature in the range of 833 - 858°C. The effect of the change in the point defect concentration on the luminescent properties of the epitaxial layers was also studied.

II. EXPERIMENTAL PROCEDURE

A. Growth Conditions

The epitaxial layers of GaP:N,S were grown on the GaP substrates by hydride VPE method. The growth was held in a vertical RF-heated reactor using the PH_3-HCl-Ga-H_2 system. The layers were doped by addition of NH_3 and H_2S to the vapour phase. The initial vapour composition was characterized by the following partial pressures:

$P^o_{H_2}$ = 0.94 atm, $P^o_{PH_3}$ = 0.006 atm, P^o_{HCl} = 0.034 atm, $P^o_{H_2S} = 2 \times 10^{-7}$ atm,

$P^o_{NH_3}$ = 0.02 atm.

At the substrate temperatures within the range of 833-858°C, the growth rate was nearly constant and equal to 0.3 μm/min. The typical thickness of the layers was about 30 μm. The depth of the nitrogen doped part was 10 μm.

The GaP substrates were grown by Liquid Encapsulated Czochralski (LEC) technique in the high-pressure crystal-pulling furnace. The substrates were oriented 4° to 7° off the (100) plane towards ⟨100⟩. The electron concentration in the substrate wafers was 2×10^{18} cm^{-3}. Prior to deposition the substrates were in situ etched in HCl at a temperature of 850°C. The substrate temperature was controlled to ±1°C by means of Pt/PtRh thermocouple and optical pyrometer.

B. Sample preparation and testing

The measurements of both electron and deep-level defect concentration were carried out using Schottky-barrier diodes as well as diodes with p^+-n junctions made by Zn diffusion. At least 10 diodes of each kind fabricated from the same epitaxial layer, grown at a given substrate temperature, were measured. Schottky barriers were formed on the epitaxial surfaces by evaporating a thin layer of Au through a mask with a 400 μm - side square opening. The Zn diffusion was carried out in an open tube at a temperature of 650°C for 22 h using a ZnO layer as the source of Zn and an SiO_2 layer as the encapsulant. The typical junction depth was 5 μm. Ohmic contacts were formed by evaporating a thin layer of Au + 1% Si on the n-type substrate surface and an array

of small Al dots on the p-type surface of the epitaxial layer. The wafer was cleaved into chips which were mounted on TO-18 transistor headers to measure junction characteristics, luminescent properties and DLTS spectra.

III. EXPERIMENTAL RESULTS AND DISCUSSION

A. DLTS spectra

The capacitance transient technique used in DLTS is based on the fact that the emission of a carrier from a deep level state is a thermally activated process characterized (for electron emission to the conduction band) by the equation [6]:

$$\tau^{-1} = e_n = \gamma_n \sigma_{na} T^2 \exp(-E_{na}/kT) \tag{1}$$

where τ is the time constant of the process and e_n is, therefore, the emission rate of electrons. E_{na} is the activation energy of electron emission, σ_{na} is the apparent capture cross-section for electrons, k is the Boltzmann constant, T is the absolute temperature and γ_n is the material constant dependent on the effective mass (for GaP $\gamma_n = 9.8\ cm^2 s^{-1} K^{-2}$).

If the capture process is accompanied by multiphonon emission then the electron capture cross-section σ_n, the apparent capture cross-section σ_{na} and the activation energy can be expressed by [6].

$$\sigma_n(T) = \sigma_{n\infty} \exp(-E_\sigma/kT), \tag{2}$$

$$\sigma_{na} = g_n \sigma_{n\infty} \exp(\Delta S_n), \tag{3}$$

$$E_{na} = E_{T0} + E_\sigma , \tag{4}$$

where E_σ is the activation energy for electron capture, $\sigma_{n\infty}$ is the limiting value of σ_n at $T \to \infty$, g_n is the degeneracy factor, ΔS_n is the entropy of the electron transition and E_{T0} is the ionisation energy extrapolated for $T \to 0$ (Gibbs free energy of the transition).

In the DLTS technique the reverse bias applied to a Schottky barier or asymmetrical junction diode is periodically pulsed to zero at a frequency f. After the reverse bias returns, those majority carriers that were captured when the depletion region collapsed will he emitted at a rate dependent upon the temperature and the energy level of the defect, according to eq. (1). The out-of-equilibrium capacitance is related to the time t by the equation [7]

$$\Delta C^* = \Delta C(t_c)\exp(-e_n t), \tag{5}$$

where t_c is the filling pulse width and $\Delta C(t_c)$ is the transient amplitude. Simple DLTS theory predicts [7] that the capacitance transient amplitude as a function of the filling pulse width is given by the following equation

$$\Delta C(t_c) = \Delta C(\infty)[1 - \exp(-t_c/\tau_1)], \tag{6}$$

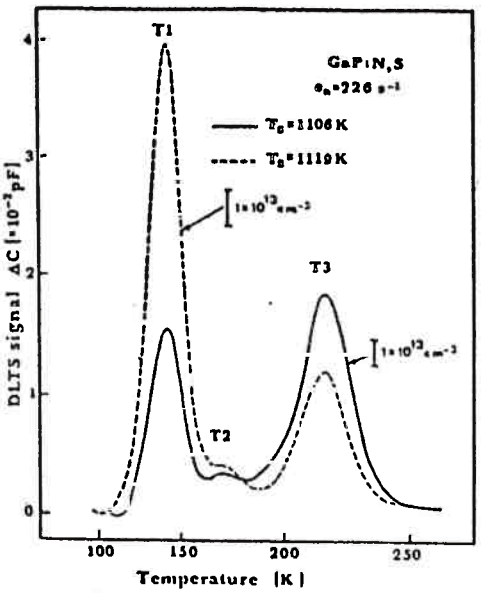

Fig. 1. DLTS spectra for epitaxial layers of GaP:N,S grown at different substrate temperatures

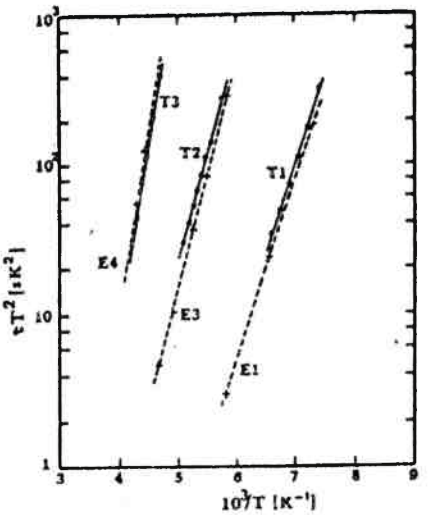

Fig. 2 Arrhenius plots for deep--level defects in VPE GaP:N,S
Broken lines are the signatures of defects reported in [8]

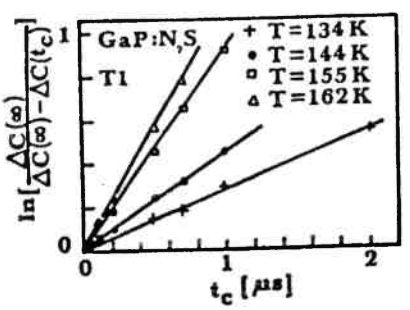

Fig. 3. Changes in the DLTS peak height versus the filling pulse width for the deep--level defect T1.
The solid lines are least--squares fits to the data measured at various temperatures.

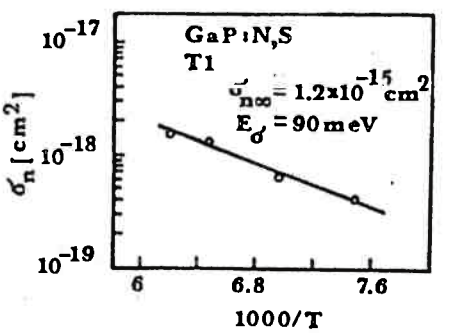

Fig. 4. Temperature dependence of electron capture cross--section for the deep-level defect T1. The actlvarlon energy for electron capture and the value of σ_n for $T \to \infty$ are given

where $\Delta C(\infty) = \Delta C(t_c \to \infty)$, $\tau_1^{-1} = \sigma_n \langle v_n \rangle n + e_n$, $\langle v_n \rangle$ is the average thermal velocity of electrons and n is the free electron concentration.

The DLTS spectra typical of the epitaxial layers of GaP:N,S grown at two different temperatures are shown in Fig. 1. The spectra were taken using a standard transient capacitance spectrometer DLS-81 at a reverse bias V_R = -4V, a filling pulse amplitude V_F = 3V and a filling pulse width t_c = 100 μs. In all samples three electron traps labelled as T1, T2 and T3 are observed. Moreover, the substrate temperature during the VPE growth has a different effect on the peak height of the two main traps T1 and T2. All the traps were characterized by drawing the Arrhenius plots of log (τT^2), versus 1/T which are shown in Fig. 2. The values of thermal emission activation energy and apparent electron capture cross-section were obtained from least-squares fits to the data according to eq. (1). The Arrhenius plots for the traps T1, T2 and T3 are compared with those reported by Tell and Kuijpers [8]. As can be seen in Fig. 2, they observed the same defect centres labelled E1, E3 and E4. However, they made no suggestion on the atomic configuration of these defects. The parameters of deep-level defects detected in VPE GaP:N,S are listed in Table 1.

Table 1.
Activation energy and apparent electron capture cross-section for deep-level defects in VPE GaP:N,S

Defect	E_{na} (eV)	$E_{na}^{*)}$ (eV)	σ_{na} (cm^2)
T1	0.24 ±0.01	0.23 (E1)	3×10^{-15}
T2	0.28 ±0.01	0.29 (E3)	5×10^{-16}
T3	0.44 ±0.02	0.47 (E4)	7×10^{-14}

*) The values reported by Tell and Kuijpers [8]

According to eq. (1) and (3) the value of σ_{na} obtained by extrapolation of the Arrhenius plots of τT^2 vs 1/T does not represent the accurate determination of σ_n. However, as it is seen from eq. (5) and (6), the capture cross-section can be measured separately by changing the duration of the filling pulse. This procedure was applied to the defect centre T1 and the results obtained are shown in Fig. 3.
The straight lines in Fig. 3 indicate that the capture process for the defect level T1 is of exponential character. The time constant τ_1 was calculated for the different temperatures from the slope of the lines and the temperature dependence of the electron capture cross-section was determined using the known carrier concentration ($n = 5 \times 10^{16} cm^{-3}$). The variations of σ_n as a function of temperature are illustrated in Fig. 4.
A least squares fit to the data according to eq. (2) gave E_σ = (90 ±10) meV and from the extrapolation for $T \to \infty$ we obtained $\sigma_{T\infty} = 1.2 \times 10^{-15} cm^2$. By taking into account eq. (4), the ionisation energy of the defect level T1 was found to be E_{T0} = 0.15 eV.

The results obtained from the investigation of capture process for the centre T1 are in good agreement with a quantitative theory of nonradiative capture by multiphonon emission (MPE) developed by Henry and Lang [9]. The theory predicts that the capture cross-sections will increase exponentially with temperature and the capture cross-sections have a common limit σ_∞ between 10^{-15} and 10^{-14} cm^2 when extrapolated to high temperatures. Because of the large electron capture cross-section, the centre T1 is likely to be an effective nonradiative recombination centre in VPE GaP.

B. Models for T1 and T3 centres

The trap T3 has been extensively studied by other investigators [10] who attempted to correlate its concentration with donor and nitrogen doping levels. A significant contribution to the understanding of the microscopic structure of the trap T3 has been made by Ferenczi et al. [11] who found an empirical formula relating the concentration of trap T3 to the electron and nitrogen concentration:

$$N_{T3} = k_1 n [N_P]^2, \tag{7}$$

where k_1 is a constant and $[N_P]$ is the nitrogen concentration. Moreover, the trap T3 was suggested to be a nitrogen split interstitial pair on phosphorus site [11].

Figure 5 shows how the concentration of defects T1 and T3 varies with the substrate temperature. The concentrations of the deep traps are proportional to the heights of the DLTS peaks and were found by means of well-known Lang's method [7]. It is seen that the T1-centre concentration strongly increases with increasing substrate temperature, while there is the opposite effect of the substrate temperature on the T3-centre concentration. In order to explain these experimental results we calculated the Ga- and P-vacancy concentrations. The calculations were performed using the following relationships [2]:

$$[V_{Ga}] = 4.85 \times 10^{-5} (P_{P_2})^{1/2} T \exp(-11920/T - 2.62 \times 10^{-5} T), \tag{8}$$

$$[V_P] = \left\{4.78 \times 10^{8} / (P_{P_2})^{1/2}\right\} \exp(-32650/T + 2.62 \times 10^{-5} T), \tag{9}$$

where $[V_{Ga}]$ and $[V_P]$ are the Ga- and P-vacancy concentrations in site fraction units, respectively, and P_{P_2} is the partial pressure of P_2 molecules over GaP. It should be noted that the model [2] which we have used for the evaluation of $[V_{Ga}]$ and $[V_P]$ assumes the Schottky mechanism for vacancy formation. It is also based on the fact that the P_2 molecules, created due to decomposition of PH_3, are the predominant phosphorus source in the gas phase [12]. The value of P_{P_2} was estimated to be 3.9×10^{-3} atm.

Figure 6 shows the T1-centre concentration plotted against calculated $[V_P]$. The straight line was fitted by the least squares method and the nearly linear relationship with the slope of 1.6 and regression coefficient of 0.99 was found. Thus, we can attribute the trap T1 to P vacancy. The main advantage of deep level transient

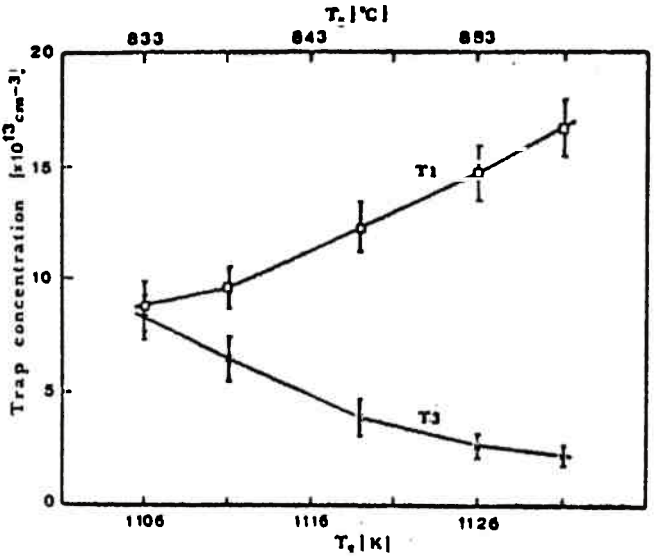

Fig. 5. Variations of the T1- and T3-centre concentrations as a function of substrate temperature

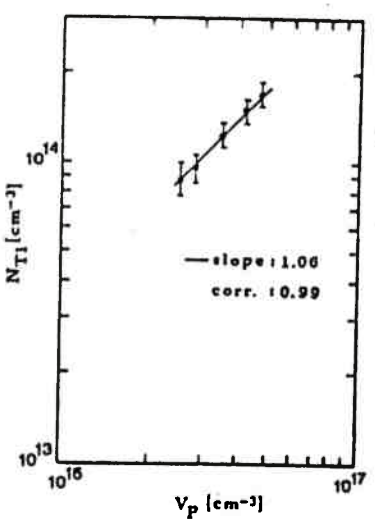

Fig. 6. Dependence of the T1-centre concentration on the calculated P-vacancy concentration. The line is a least squares fit to the data

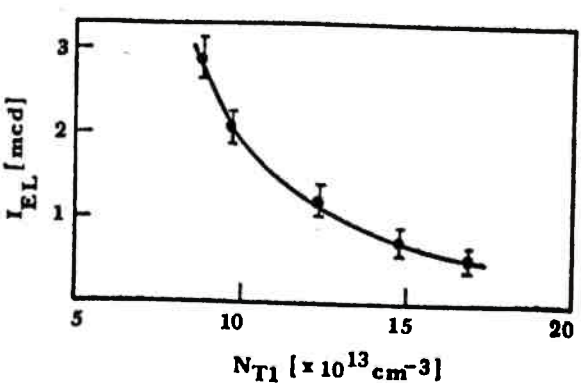

Fig. 7. Variation of the luminous intensity of VPE GaP:N,S light emitting diodes as a function of the T1-centro concentration

spectroscopy is that it enables one to correlate the quantum efficiency of LEDs with the presence of deep defect centres. The relationship between the luminous intensity of the LEDs fabricated from the epitaxial layers grown at various substrate temperatures and the T1-centre concentration is shown in Fig. 7. This relationship confirms our previous suggestions made on the grounds of the capture process studies and it is clearly seen that the defect centre T1 has a detrimental effect on the radiative recombination efficiency in VPE GaP. In the light of the fact that the trap T1 is related to P vacancy, the results in Fig. 7 give the evidence, that P vacancies, similarly as Ga vacancies, are efficient nonradiative recombination centres.

CONCLUSIONS

DLTS measurements were performed on VPE GaP:N,S LEDs and Schottky barriers fabricated from the epitaxial layers grown at various substrate temperature. In all samples we found three trap levels in the upper half of the forbidden gap:T1 (0.24eV). T2 (0.28eV) and T3 (0.44eV).

The capture process for the trap T1 was studied. The activation energy for electron capture and the limiting value of electron capture cross-section were found to be E_σ = 90meV and $\sigma_{n\infty} = 1.2 \times 10^{-15}$ cm^2, respectively. These results are consistent with those predicted by a theory of MPE capture.

A correlation between the T1-centre concentration and the calculated P-vacancy concentration as a function of substrate temperature has been found. The experimental evidence is given that the defect centre T1 has a detrimental effect on the luminescent properties of VPE GaP:N,S.

BIBLIOGRAPHY

1. Thomas D.G., Hopfield J.J.: Phys. Rev. 150 (1966), 680
2. Jordan A.S., Caruso R., Von Neida A.R., Weiner M.E.: J. Appl. Phys. 45 (1974), 3472
3. Fabre E., Bhargava, R.N.: Appl. Phys. Letters 24 (1974), 322
4. Bhargava R.N., Kurtz S.K., Vink A.T., Peters R.C.: Phys. Rev. Letters 27 (1971), 183
5. Stringfellow G.B., Hall H.T.: J. Electrochem. Soc. 123 (1976), 916
6. Look D.C., in Semiconductors and Semimetals, edited by R.K. Willardson and A.C. Beer (Academic Press, New York 1983), Vol. 19, p. 76
7. Lang D.V.: J. Appl. Phys. 45 (1974), 3023
8. Tell B., Kuijpers F.P.J.: J. Appl. Phys. 49 (1978), 5938
9. Henry C.H., Lang D.V.: Phys. Rev. B 15 (1977) 989
10. Wessels B.W.: J. Appl. Phys. 48 (1977), 1656
11. Ferenczi G., Krispin P., Somogyi M.: J. Appl. Phys. 54 (1983), 3902
12. Epstein A.S.: J. Phys. Chem. Solids 27 (1966), 1611

Artykuł opublikowano w materiałach z konferencji: IX Szkoła Fizyki i Zastosowań Nadkryształów i Materiałów..., Jurata 1990

K. MAZUR, J. SASS, M. BERKOWSKI*
INSTYTUT TECHNOLOGII MATERIAŁÓW ELEKTRONICZNYCH
ul. Wólczyńska 133, 01-919 Warszawa
*INSTYTUT FIZYKI, POLSKA AKADEMIA NAUK
al. Lotników 32, 02-668 Warszawa

THE INVESTIGATION OF DEFECTS IN $LaGaO_3$ SINGLE CRYSTAL

We do research on $LaGaO_3$ single crystal. It is a promising new material for epitaxial high temperature superconducting thin film. $LaGaO_3$ crystal has an orthorhombic structure with lattice parameters a = 0,5519 nm, b = 0,5494 nm, c = 0,777 nm and belongs to Rare Earth Gallium Perovskites. $LaGaO_3$ is isomorphic to $GdFeO_3$ but its ion coordinates at the unit cell are unknowned. Therefore the structure of $LaGaO_3$ is described in terms of distorted perovskite cell. There are four distorted perovskite cells in the orthorhombic unit cell.
The defects of crystal structure were investigated by means of X-ray diffraction topography. The crystal plates were cut perpendicullar to the growth axies [011]. It was established occuring the longitudinal volume defects. There are two kinds of these defects:

1 - where the areas of defects are limited by crystallographic plane (112) inclined about 35° to the (011) plane,
2 - where the areas of defects are limited by crystallographic plane ($1\bar{1}2$) perpendicullar to the (011) plane.

The crystallographic interpretation of these defects has been presented.

Wystąpienie opublikowano w materiałach z konferencji: IX Szkoła Fizyki i Zastosowań Monokryształów ..., Jurata 1990

J. GACA, M. WÓJCIK, J. SASS
INSTYTUT TECHNOLOGII MATERIAŁÓW ELEKTRONICZNYCH
ul. Wólczyńska 133, 01-919 Warszawa

DOUBLE MODULATION WAVE IN InGaAs/AsP CRYSTALS

The investigated samples were made by MOCVD technique and were grown is such a way that their structure can be regarded as having a unit cell which is very large in h00 direction. It can be seen as consisting of two parts, differing as well in lattice constanc as in their thicknesses. In the first part there are two kinds of planes- the Ga planes with the planar structure factor f_{Ga} - and - As-P planes with f_{As-P} placed alternately at the distance $\frac{a}{4}$ where a - the lattice constant of the first part. The second part is similar to the first one, the only difference consists in replacing the Ga planes by Ga-In ones and the As-P planes by As ones with appropriate structure factors. This kind of structure when investigated difractometrically in the h00 direction give rise to satellites accompanying the main reflection peak. The positions of the satellites in reciprocal space are determined by the period of the modulation.

Wystąpienie opublikowano w materiałach z konferencji: IX Szkoła Fizyki i Zastosowań Monokryształów ..., Jurata 1990

J. SASS, J. GACA, M. WÓJCIK
INSTYTUT TECHNOLOGII MATERIAŁÓW ELEKTRONICZNYCH
ul. Wólczyńska 133, 01-919 Warszawa

THE SINUSOIDAL MODULATION WAVE MODEL APPLIED TO THE BINARY ALLOYS

Samples of Ti-containing Alnico alloy in the high coercive state were subjected to an X-ray diffractometric investigations. Two surfaces of the samples were investigated: one parallel and the second perpendicular to the lines of the forces of the external magnetic field $\vec{H}$. The investigations showed that the alloy had the structure of an ordered solid solution with cubic body centered lattice $\langle a \rangle = 0{,}2873 \pm 0{,}0003$ nm, where $\langle a \rangle$ is an average value of the parameter a. There is the superstructure of the CsCl type. There is a periodic modulation of the interplanar spacing and scattering power in the direction perpendicular to the forces lines of the external magnetic field $\vec{H}$. It is supposed that this periodic modulation is caused by a periodic modulation is caused by a periodic variation of the composition - there is a higher concentration of Al-atoms in the region where $a_1 < \langle a \rangle$ and a higher concentration of Fe-atoms in the region, where $a_2 < \langle a \rangle$.

Wystąpienie opublikowano w materiałach z konferencji: IX Szkoła Fizyki i Zastosowań Monokryształów ..., Jurata 1990

M. WÓJCIK, J. GACA, J. SASS
INSTYTUT TECHNOLOGII MATERIAŁÓW ELEKTRONICZNYCH
ul. Wólczyńska 133, 01-919 Warszawa

THE SUPERLATTICE MODEL WITH COHERENT SCATTERING DOMAINS

The model of the distribution of modulation wave-length around some average value brought about by a chemical gradient across the sample was accepted and experimentally checked. This model implies dividing the crystal into coherent scattering domains (CSD). In each CSD the composition modulation wave can be described by means of the sinusoidal wave. The wave-length in each CSD is constant and may be different from one to another. The variation of the composition in each CSD is coupled with structure factor and lattice constant modulation. The CSD's are separated by the boundaries in such a way, that there is no long range order in the lateral direction of the crystal. This model implies that the half width of the satellite reflections accompaining the main peakare broadenedin comparision to the ones in the ideal SL model.

Wystąpienie opublikowano w materiałach z konferencji: IX Szkoła Fizyki i Zastosowań Monokryształów ..., Jurata 1990

Z. FRUKACZ, J. KISIELEWSKI, Z. MIERCZYK*, W. SZYRSKI
INSTYTUT TECHNOLOGII MATERIAŁÓW ELEKTRONICZNYCH
ul. Wólczyńska 133, 01-919 Warszawa

*INSTYTUT ELEKTRONIKI KWANTOWEJ WAT
ul. Kaliskiego , 00-908 Warszawa

OTRZYMYWANIE I WŁASNOŚCI OPTYCZNE MONOKRYSZTAŁU Ti:Al_2O_3

WSTĘP

W 1982 r. Moulton (MIT, Lincoln Lab.) uzyskał po raz pierwszy akcję laserową na monokrysztale Ti:Al_2O_3. Od tego czasu nastąpiło wielkie zainteresowanie tym kryształem ze względu na możliwość wykorzystania go do budowy laserów przestrajalnych w szerokim paśmie od ok. 660 nm do ponad 1000 nm.

Kryształ Al_2O_3 domieszkowany trójwartościowym tytanem ma ciemnoróżowe zabarwienie spowodowane szerokim pasmem absorpcji w widzialnym obszarze widma 400 ÷ 600 nm. Maksimum absorpcji występuje dla długości fali 490 nm. Wzbudzenie optyczne kryształu światłem zielono-żółtym wywołuje luminescencję w paśmie 600 ÷ 1050 nm z maksimum dla ok. 750 nm. W tym paśmie Moulton uzyskał akcję laserową o przestrajalnej długości fali emitowanej 660 ÷ 990 nm [1].

W podczerwieni występuje szerokie pasmo stosunkowo słabej absorpcji z maksimum dla długości fali ok. 850 nm. Ta szczątkowa absorpcja jest spowodowana obecnością w krysztale jonów Ti^{4+} i jest proporcjonalna do ich koncentracji. Ponieważ pasmo absorpcji w podczerwieni obejmuje cały obszar pasma luminescencji, to absorpcja w tym obszarze jest niekorzystna, gdyż tłumi emisję i obniża sprawność lasera.

Jako wielkość charakteryzującą jakość kryształu (Figure of Merit - FOM) przyjmuje się stosunek wartości współczynnika absorpcji dla długości fali odpowiadającej maksimum pasma pompowania do wartości współczynnika absorpcji dla długości fali odpowiadającej maksimum pasma pochłaniania w podczerwieni. Stosunek ten powinien mieć wartość jak najwyższą. Okoliczność ta powoduje, że zasadniczym problemem dla technologii jest uzyskanie monokryształu z jak najmniejszą koncentracją jonów Ti^{4+}. W najlepszych wytwarzanych kryształach ilość jonów Ti^{3+}, przed wygrzewaniem w atmosferze wodoru, wynosi do 3% wszystkich atomów tytanu [4].

Celem naszej pracy, której wstępne wyniki tu przedstawimy, jest wytwarzanie w kraju bardzo ważnego współcześnie materiału laserowego.

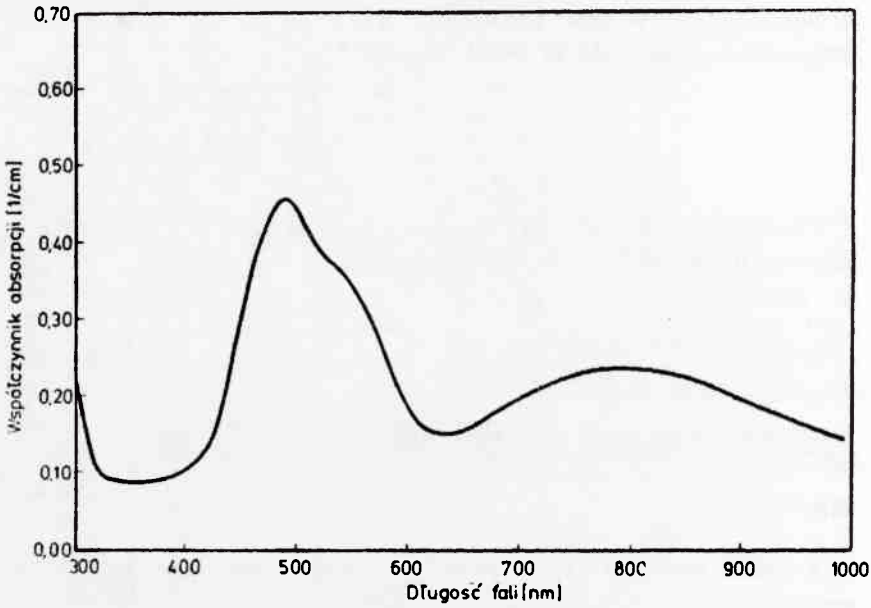

Rys. 1. Widmo absorpcji próbki nr 1 monokryształu Ti:Al_2O_3. Wartość współczynnika FOM wynosi 2,0

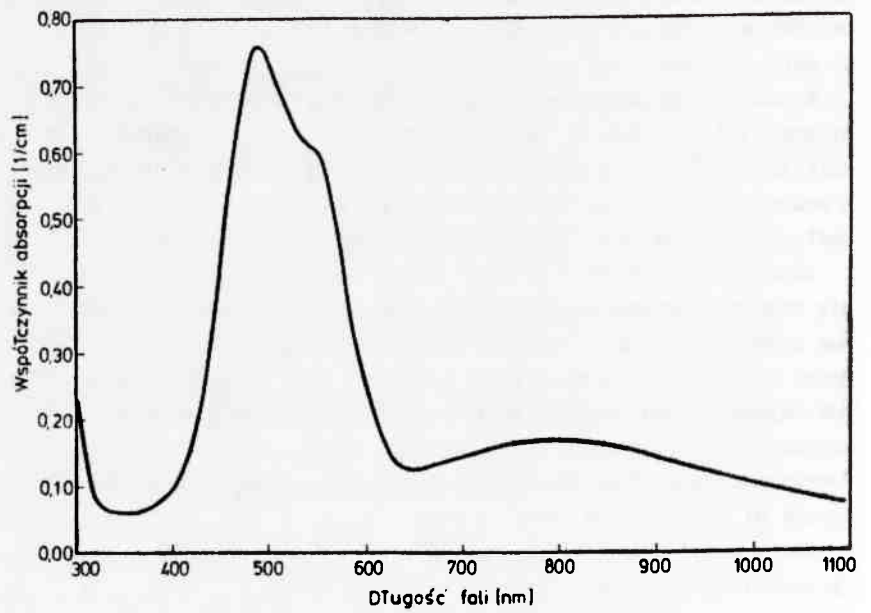

Rys. 2. Widmo absorpcji próbki nr 2 monokryształu Ti:Al_2O_3. Wartość współczynnika FOM wynosi 4,7

MONOKRYSTALIZACJA

Proces wzrostu monokryształu był prowadzony metodą Czochralskiego z użyciem tygla irydowego grzanego indukcyjnie. Zarodek był wykonany z monokryształu leukoszafiru (czystego Al_2O_3) i zorientowany tak, że krystalograficzna oś c była prostopadła do geometrycznej osi zarodka. Prędkość wzrostu monokryształu wynosiła ok. 0,8 mm/h.

Liczba jonów Ti^{4+} w monokryształe rośnie wraz ze wzrostem ciśnienia parcjalnego tlenu w atmosferze krystalizacji. Na tym etapie pracy zrezygnowaliśmy z wprowadzenia do komory krystalizacyjnej wodoru oraz stosowania geterów tlenowych. Beztlenowa atmosfera była zapewniona przez następujące warunki:

- krystalizacja przebiegała w szczelnej komorze napełnionej azotem o wysokiej czystości (maks. 2 ppm O_2, 2 ppm H_2O),
- do domieszkowania użyto Ti_2O_3 zamiast TiO_2, który w temperaturze powyżej 1750°C przechodzi w Ti_2O_3 z wydzielaniem się wolnego tlenu wg reakcji:

$$2TiO_2 \rightarrow Ti_2O_3 + \frac{1}{2} O_2,$$

- przed rozpoczęciem krystalizacji komora była starannie oczyszczona z tlenu przepływającym azotem.

Do napełniania tygla użyte zostały: trójtlenek tytanu Ti_2O_3 (firmy Merck o czystości 3N) oraz złom krystaliczny Al_2O_3 (powstały przy produkcji kryształów leukoszafiru metodą Verneuile'a, o czystości ok. 5N).

Rozpuszczalność tlenku tytanu w roztopionym Al_2O_3 jest mała i nie przekracza 1% wagowego [3]. Przygotowane zostały dwa wsady o zbliżonym stężeniu: 0,92% i 0,98% wag. Ti_2O_3. Na skutek znacznej różnicy promieni jonowych atomów glinu i tytanu, które dla Al^{3+}, Ti^{3+} i Ti^{4+} wynoszą odpowiednio 0,51; 0,76 i 0,68 Å, wbudowywanie się jonów tytanu do sieci korundu jest utrudnione i w efekcie w rosnącym krysztale będzie mniej tytanu niż w roztopie w tyglu. Ilościowo różnicę tę określa współczynnik segregacji $K = C_S/C_e = 0,11$ [2].

Na podstawie tego współczynnika segregacji możemy określić koncentrację Ti_2O_3 w otrzymywanych przez nas kryształach na 0,1% wag., co odpowiada koncentracji $[Ti] = 3 \times 10^{19}$ cm^{-3}.

Przeprowadzono pięć procesów krystalizacji, uzyskano cztery kryształy o wymiarach: średnica 15÷24 mm, długość 25÷55 mm. Wszystkie kryształy były obustronnie symetrycznie spłaszczone, co świadczy o dobrej ich orientacji (oś c prostopadła do osi kryształu). Intensywne różowe zabarwienie, równomierne w całej objętości kryształów, świadczy o dużej zawartości jonów Ti^{3+} i równomiernym ich rozmieszczeniu. Występowanie pęcherzy, charakterystyczne dla krystalizacji Al_2O_3, jest skutkiem powstawania przechłodzenia na froncie krystalizacji. Mała liczba przeprowadzonych prób uniemożliwiła dobranie optymalnych warunków monokrystalizacji (gradient temperatury na froncie krystalizacji, prędkość wyciągania i inne) zapewniających otrzymanie kryształów wolnych od pęcherzy.

Z obszarów pozbawionych pęcherzy wycięto kilka próbek, dla których wyznaczono widmo absorpcji (rys. 1, 2) oraz widmo luminescencji (rys. 3).

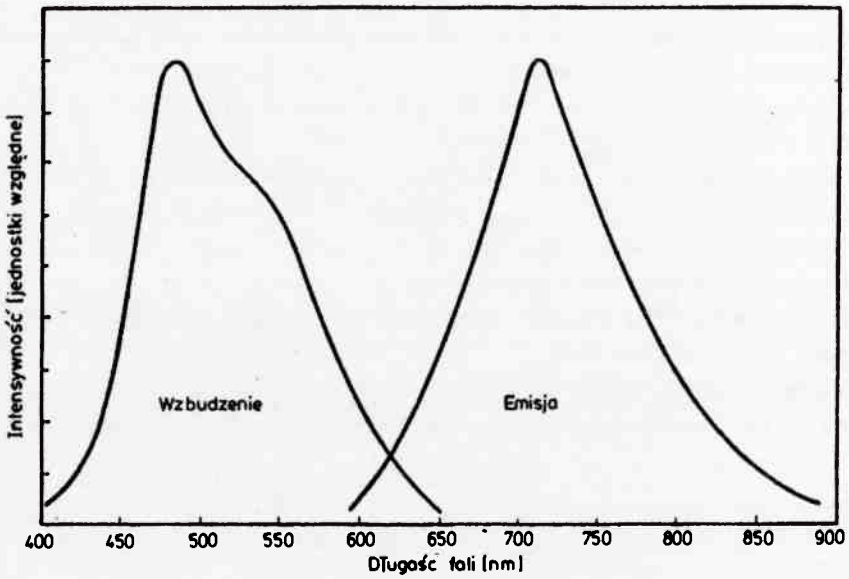

Rys. 3. Widmo emisji i wzbudzenia próbki nr 2 monokryształu $Ti:Al_2O_3$

WYNIKI BADAŃ SPEKTROSKOPOWYCH

W celu wyznaczenia współczynnika absorpcji $Ti:Al_2O_3$ w funkcji długości fali, przeprowadzono badania transmisji próbek w zakresie widmowym 200 ÷ 1100 nm na spektrofotometrze LAMBDA-2 firmy PERKIN - ELMER.

Zależność $\alpha(\lambda)$ wyznaczono na podstawie pomiaru transmisji $T(\lambda)$, uwzględniając wielokrotne odbicia promieniowania od powierzchni próbek $Ti:Al_2O_3$.

Obliczenia przeprowadzono dla transmisji rzeczywistej $T_r(\lambda)$ związanej z transmisją zmierzoną $T(\lambda)$ zależnością:

$$T(\lambda) = \frac{(1 - r_f)^2 T_r}{1 - T_r^2 r_f^2}$$

gdzie: r_f - fresnelowski współczynnik odbicia $Al_2O_3:Ti$

$$r_f = \frac{(n - 1)^2}{(n + 1)^2}$$

n - współczynnik załamania światła $Al_2O_3:Ti$.

Wykorzystano następującą formułę dyspersyjną [5]:

$$n^2 - 1 = \frac{A_1 \lambda^2}{\lambda^2 - \lambda_1^2} + \frac{A_2 \lambda^2}{\lambda^2 - \lambda_2^2} + \frac{A_3 \lambda^2}{\lambda^2 - \lambda_3^2}$$

gdzie:

$\lambda_1 = 0{,}06144821$ $\quad A_1 = 1{,}023798$

$\lambda_2 = 0{,}1106997$ $\quad A_2 = 1{,}058264$

$\lambda_3 = 17{,}92656$ $\quad A_3 = 5{,}280792$

Rzeczywista transmisja badanej próbki wynosi:

$$T_r = \frac{-(1 - r_f)^2 + \sqrt{(1 - r_f)^4 + 4 r_f^2 T^2}}{2 T r_f^2}$$

Współczynnik absorpcji obliczono wg zależności:

$$\alpha(\lambda) = \frac{1}{l} \ln \frac{1}{T_r(\lambda)}$$

gdzie: l - długość próbki.

Przykładowe wyniki obliczeń zależności $\alpha(\lambda)$ dla dwóch próbek $Ti:Al_2O_3$ przedstawiono na rysunkach 1 i 2.

Obliczony stosunek współczynników absorpcji dla długości fal 490 nm i 850 nm [3], charakteryzujący jakość monokryształu $Ti:Al_2O_3$, wynosi dla próbki 1 (rys. 1):

$$\frac{\alpha(490\ nm)}{\alpha(850\ nm)} = 2{,}0,$$

dla próbki 2 (rys. 2):

$$\frac{\alpha(490\ nm)}{\alpha(850\ nm)} = 4{,}7.$$

Na rys. 3 przedstawiono widma emisji i wzbudzenia próbki $Ti:Al_2O_3$. Badania przeprowadzono na spektrofluorymetrze PERKIN-ELMER LS-5B. Analizowany kryształ charakteryzuje szerokie pasmo wzbudzenia (400 ÷ 650 nm) z maksimum 485 nm oraz pasmo emisji 650 ÷ ok. 900 nm z maksimum 713 nm.

WNIOSKI KOŃCOWE

1. Opracowana technologia monokrystalizacji umożliwia uzyskanie kryształów $Ti:Al_2O_3$ o własnościach spektralnych zapewniających generację promieniowania w szerokim zakresie widmowym od 650 nm do ok. 900 nm.
2. Mała wartość współczynnika absorpcji w obszarze pompowania wynika z niskiej zawartości jonów Ti^{3+} w sieci krystalicznej Al_2O_3, co jest rezultatem niestosowania atmosfery redukującej w komorze monokrystalizacyjnej.
3. Absorpcja w podczerwieni wynika z występowania w strukturze uzyskanych kryształów mikropęcherzy charakterystycznych dla krystalizacji Al_2O_3. Efekt ten jest skutkiem powstawania przechłodzenia na froncie krystalizacji. Mała liczba przeprowadzonych prób uniemożliwiła dobranie optymalnych warunków monokrystalizacji (gradient temperatury na froncie krystalizacji, prędkość wyciągania i inne) zapewniających otrzymanie kryształów wolnych od mikropęcherzy.

LITERATURA

1. Moulton P.F.: Spectroscopic and laser characteristics of Ti:Al_2O_3, J. Opt. Soc. Amer. B, vol 3, pp. 125-133, 1986
2. Kokta M.: Growth of Titanium Doped Sapphire, Topical Meeting on Tunable Solid-State Lasers, May 16-17, 1985, Arlington, Virginia
3. Lacovara P., Estarowitz L., Kokta M.: Growth, Spectroscopy and Lasing of Titanium-oped Sapphire, IEEE J. Quantum Electron., vol. QE-21, pp. 1614-1618, 1985
4. Sanchez A., Strauss A.J., Aggarwal R.L., Fahey R.E.: Crystal Growth, Spectroscopy and Laser Characteristic of Ti:Al_2O_3, IEEE J. Quantum Electron., vol QE-24, pp. 995-1002, 1988
5. Katalog Harshaw optical crystals, The Harshaw Chemical Company, Cleveland, 1967